MODELING AND SIMULATION OF ELECTRON TRANSPORT AND HEATING IN SEMICONDUCTOR DEVICES AND CIRCUITS

Ansgar Jüngel[1]
[1]Vienna University of Technology, Institute for Analysis and Scientific Computing,
Wiedner Hauptstraße 8-10, 1040 Wien, Austria, juengel@anum.tuwien.ac.at

Corresponding author: Ansgar Jüngel

Abstract. In this review, thermal effects in semiconductor devices and electric circuits are modeled and numerically simulated. The device heating is due to the particle temperatures, recombination effects, and the thermal power from the companion thermal network. The complete model consists of the energy-transport equations for the charge carriers and the particle temperatures in the semiconductor device, together with a heat equation for the lattice temperature; the electric network equations; and the thermal network describing the heat evolution in the circuit elements. The derivation of the energy-transport equations from the semiconductor Boltzmann equation is sketched, and the submodels and their couplings are introduced. The heating effects are illustrated by several numerical examples.

AMS Subject Classification: 65L80, 65M60, 65N30, 80A20, 82D37.

1 Introduction

Self-heating is becoming of paramount importance in modern ultra-integrated circuits and power devices since it influences strongly the circuit behavior or even lowers its performance. The standard approach for the modeling of integrated circuits is to replace the semiconductor devices by equivalent circuits consisting of basic elements and including (thermal) fitting parameters. Due to the decreasing feature size and increasing operating frequency, however, a very large number of basic elements and a careful adjustment of the large number of fitting parameters is needed in order to achieve the required accuracy. Therefore, it is preferable to model thermally relevant semiconductor devices by transport equations and to develop a coupled model for the particle temperatures, the lattice temperature in the device, and the temperatures of the circuit elements. The goal of this paper is to review the derivation of the energy-transport equations and the modeling of electric circuits and thermal networks and to present some numerical examples illustrating the self-heating behavior.

Thermal effects in microelectronic modeling were already considered in the 1970s [1, 26]. First coupled circuit-device models were often based on a combination of device and circuit simulators [23]. More recently, electric network models were coupled to semiconductor transport equations, using drift-diffusion [43, 47] or energy-transport models [3, 13]. A thermodynamic approach to extend the drift-diffusion equations to the nonisothermal case was presented in [49], later generalized in [2] using first principles of entropy maximization and partial local equilibrium. Recently, an energy-transport model coupled to electric circuit equations and a lattice heat equation was numerically simulated in [14].

Self-heating is described by the following models. First, the energy-transport equations allow for the computation of the particle temperatures. Collisions of the charge carriers with the crystal lattice (modeled by a relaxation-time ansatz) leads to an increasing lattice temperature which is described by a heat equation derived from thermodynamic principles. Second, the circuit is modeled by electric network equations resulting from the so-called modified nodal analysis. Third, a thermal network model describes the heat evolution in the (lumped and distributed) circuit elements. These three subsystems are coupled by thermoelectric, electric circuit-device, and thermal network-device interfaces. Figure 1 presents an overview of the subsystems.

In Section 2 we introduce the energy-transport equations for the electrons. First their derivation from the semiconductor Boltzmann equation is sketched. The equations are numerically approximated by using mixed finite-element methods, and numerical simulations of two- and three-dimensional devices are presented. The equation for the lattice temperature is derived in Section 3. Section 4 is concerned with the modeling of the electric circuit employing the Kirchhoff laws and current-voltage characteristics of the

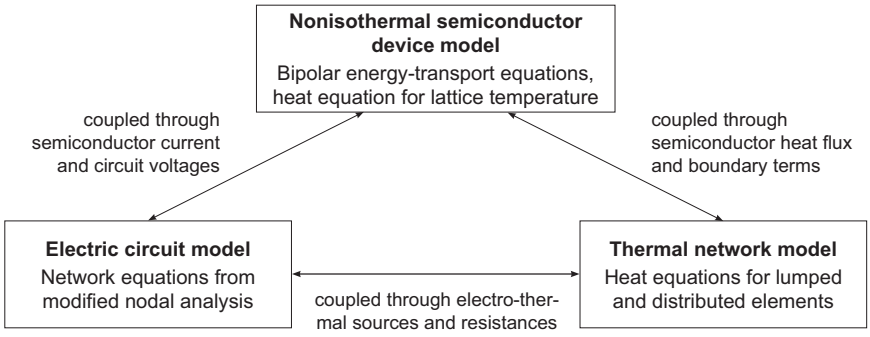

Figure 1: Overview of the coupled thermo-electric circuit-device model.

basic elements. Thermally relevant circuit elements are described in a thermal network model detailed in Section 5. Finally, the fully coupled model is considered in Section 6.

2 Energy-transport modeling

Heating of electrons in the semiconductor crystal is described by the energy-transport equations. In this section, we sketch its derivation from the semiconductor Boltzmann equation, approximate the equations numerically, and present some numerical examples.

2.1 Derivation of the model

The semiconductor crystal is supposed to be a three-dimensional array of atoms arranged in a lattice. The quantum states of the electrons in the periodic lattice are given by the eigenfunctions $\psi_n(k)$, $n \in \mathbb{N}$, of a suitable Schrödinger equation, indexed by the so-called pseudo-wave vector $k \in B$, where the subset $B \subset \mathbb{R}^3$ is the Brillouin zone (see [33, 35] for details). The corresponding eigenvalue $E(k) = E_n(k)$ represents the energy of the state k in the n-th band.

Instead of a full quantum description, we prefer a semi-classical model in which the electrons in the conduction band are modeled statistically and quantum effects enter only through the (conduction) band structure $E(k)$. Let $f(x,k,t)$ be the distribution function of an electron ensemble, where $x \in \mathbb{R}^3$ denotes the spatial variable and $t > 0$ the time. More precisely, $f(x,k,t)$ is the ratio of the number of occupied quantum states of the electrons in the infinitesimal volume element $dx\,dk$ in the conduction band to the total number of states in $dx\,dk$ in the conduction band. The distribution function $f_\alpha(x,k,t)$ is assumed to satisfy the scaled semiconductor Boltzmann equation

$$\alpha^2 \partial_t f_\alpha + \alpha\big(v(k)\cdot\nabla_x f_\alpha + \nabla_x V\cdot\nabla_k f_\alpha\big) = Q(f_\alpha), \quad x \in \mathbb{R}^3,\ k \in B,\ t > 0,$$

where $\alpha > 0$ is the (scaled) mean free path of the particles, $v(k) = \nabla_k E(k)$ the electron group velocity, $V = V(x,t)$ the electric potential, and $Q(f)$ is the collision operator. The Boltzmann equation is complemented with periodic boundary conditions for $k \in B$ and initial conditions for f. The collision operator is decomposed as the sum of elastic, electron-electron, and inelastic scattering terms according to

$$Q(f) = Q_{\mathrm{el}}(f) + \alpha Q_{\mathrm{ee}}(f) + \alpha^2 Q_{\mathrm{in}}(f).$$

We do not make precise the structure of the scattering terms since we need only some properties (and refer to [33] for details): The kernel of the linear elastic collision operator Q_{el} consists of functions which depend only on the energy, $f(x,k,t) = F(x,E(k),t)$. Furthermore, the kernel of the electron-electron collision operator Q_{ee} consists of Fermi-Dirac distributions, $f = (1+\exp((E(k)-\mu)/T_n))^{-1}$, where the chemical potential $\mu \in \mathbb{R}$ and the electron temperature $T_n > 0$ are some parameters. Moreover, we assume that scattering conserves mass and that elastic scattering additionally conserves energy:

$$\int_B Q_\gamma(f)\,dk = \int_B Q_{\mathrm{el}}(f)E\,dk = 0 \quad \text{for all } f,\ \gamma = \mathrm{el}, \mathrm{ee}, \mathrm{in}.$$

We suppose that the mean free path is "small", $\alpha \ll 1$, meaning that we consider a time scale much larger than the typical time between two inelastic collisions. We refer to [33] for the precise scaling.

The main idea of the derivation of the macroscopic equations is to multiply the Boltzmann equation by 1 and $E(k)$, to integrate the resulting equation over the wave-vector space, which leads to the so-called moment equations

$$\partial_t \int_B f_\alpha dk' + \frac{1}{\alpha}\mathrm{div}_x \int_B f_\alpha v dk' = 0, \tag{1}$$

$$\partial_t \int_B f_\alpha E dk' + \frac{1}{\alpha}\mathrm{div}_x \int_B f_\alpha v E dk' - \frac{1}{\alpha}\nabla_x V \cdot \int_B f_\alpha v dk' = \frac{1}{\alpha^2}\int_B Q(f_\alpha) E dk', \tag{2}$$

where $dk' = dk/4\pi^3$, and to perform the (formal) limit $\alpha \to 0$ appropriately.

The derivation consists of three steps, following [22]. In the first step, we let formally $\alpha \to 0$ in the Boltzmann equation leading to $Q_{\mathrm{el}}(f) = 0$, where $f = \lim_{\alpha\to 0} f_\alpha$. Thus, $f(x,k,t) = F(x,E(k),t)$ for some function F. For the second step, we insert the Chapman-Enskog expansion $f_\alpha = F + \alpha g_\alpha$ (which defines g_α) into the Boltzmann equation and let $\alpha \to 0$:

$$Q_{\mathrm{el}}(g) = v(k)\cdot\nabla_x F + \nabla_x V \cdot \nabla_k F - Q_{\mathrm{ee}}(F),$$

where $g = \lim_{\alpha\to 0} g_\alpha$. It can be shown that this operator equation is formally solvable if and only if its integral over the energy surface of energy ε vanishes [33], which, after some manipulations, can be written as

$$\int_B Q_{\mathrm{ee}}(F)\delta(E(k)-\varepsilon)dk = 0 \quad \text{for all } \varepsilon.$$

The integral involving the delta distribution can be mathematically defined by using the coarea formula. By assumption, F is a Fermi-Dirac distribution, $F = F_{\mu,T_n} = (1+\exp((E(k)-\mu)/T_n))^{-1}$ for some $\mu = \mu(x,t)$ and $T_n = T_n(x,t)$.

The third step is concerned with the limit $\alpha \to 0$ in the moment equations (1)-(2). The integral of F_{μ,T_n} over B vanishes since $v = \nabla_k E$ and F_{μ,T_n} lies in the kernels of Q_{el} and Q_{ee}. Thus, the α^{-1}-terms in (1)-(2) vanish and the moment equations become in the limit

$$\partial_t \int_B F_{\mu,T_n} dk' + \mathrm{div}_x \int_B g v dk' = 0,$$

$$\partial_t \int_B F_{\mu,T_n} E dk' + \mathrm{div}_x \int_B g v E dk' - \nabla_x V \cdot \int_B g v dk' = \int_B Q_{\mathrm{in}}(F_{\mu,T_n}) E dk'.$$

Introducing the electron and energy densities and the particle and energy current densities

$$n = \int_B F_{\mu,T_n} dk', \quad ne = \int_B F_{\mu,T_n} E dk', \quad J_n = -\int_B g v dk', \quad S_n = -\int_B g v E dk', \tag{3}$$

respectively, the moment equations can be formulated as

$$\partial_t n - \mathrm{div}_x J_n = 0, \quad \partial_t(ne) - \mathrm{div}_x S_n + \nabla_x V \cdot J_n = W, \tag{4}$$

where $W = \int_B Q_{\mathrm{in}}(F) E dk'$. In order to derive expressions for the current densities which depend on the macroscopic variables, we introduce the vector-valued solution d_0 of $Q_{\mathrm{el}}(d_0) = -vF(1-F)$. Then, since $F = (1+\exp((E(k)-\mu)/T_n))^{-1}$ and since Q_{el} is assumed to be linear, we can write $g = -d_0 \cdot (\nabla_x(\mu/T_n) - \nabla_x V/T - E\nabla_x(1/T_n)) + F_1$, and F_1 lies in the kernel of Q_{el}. This implies that

$$J_n = D_{00}\Big(\nabla_x \frac{\mu}{T_n} - \frac{\nabla_x V}{T_n}\Big) - D_{01}\nabla_x\Big(\frac{1}{T_n}\Big), \quad S_n = D_{10}\Big(\nabla_x \frac{\mu}{T_n} - \frac{\nabla_x V}{T_n}\Big) - D_{11}\nabla_x\Big(\frac{1}{T_n}\Big), \tag{5}$$

and the diffusion coefficients are given by

$$D_{ij} = D_{ij}(\mu, T_n) = \int_B E^{i+j} v \otimes d_0 dk, \quad i,j = 0,1. \tag{6}$$

The functions (n, ne) and (μ, T_n) are related by the first two equations in (3). Equations (4)-(6) are referred to as the *energy-transport equations*. They are complemented by initial conditions for n and T_n and, in the case of a bounded domain, by mixed Dirichlet-Neumann or Robin-Neumann boundary conditions for n, T_n, and V (see [13]).

Another contribution to the current flow is due to defect electrons in the valence band, which are usually described by pseudo-particles: holes. Physically, a hole is a vacant orbital in a valence band. Also for these particles, an energy-transport model for the hole density p and the hole temperature T_p (with the hole current density J_p and the hole energy flux S_p) can be derived. Often, the hole temperature can be approximated by the lattice temperature, and the hole density evolves according to the drift-diffusion model

$$\partial_t p + \operatorname{div} J_p = -R(n,p), \quad J_p = -\nabla(\mu_p p) - \mu_p p \nabla V, \tag{7}$$

where μ_p is the hole mobility and $R(n,p)$ describes recombination-generation processes between electrons and holes.

The above transport equations are coupled to the Poisson equation for the electric potential:

$$\lambda^2 \Delta V = n - p - C(x), \tag{8}$$

where λ is the (scaled) Debye length and $C(x)$ the doping profile modeling fixed background charges in the semiconductor crystal.

The first energy-transport model was presented by Stratton in 1962 [45]. Often, the energy-transport model is considered as an approximation of the hydrodynamic equations [42]. There are only a few mathematical results about the initial-value problem of the energy-transport equations, since they are strongly coupled. The first existence result for a heuristic model was proved in [4]. Existence results for models with a uniformly positive diffusion matrix were shown in [19, 20] and for data close to equilibrium in [18, 24, 28].

In nonequilibrium thermodynamics, the formulation (4)-(5) is well known. Indeed, the so-called thermodynamic fluxes depend linearly on the thermodynamic forces $X_0 = \nabla(\mu/T_n) - \nabla V/T_n$ and $X_1 = -\nabla(1/T_n)$ [29]. The variables μ/T_n and $-1/T_n$ are known as the (primal) entropy variables. The connection to thermodynamics has an important consequence. By introducing the dual entropy variables $w_0 = (\mu - V)/T_n$ and $w_1 = -1/T_n$, the current densities can be written in the "symmetric" form

$$J_n = \sum_{i=0}^{1} L_{0i} \nabla w_i, \quad S_n = \sum_{i=0}^{1} L_{1i} \nabla w_i, \tag{9}$$

where the new diffusion coefficients L_{ij} depend on D_{ij} and V, and the equation for the energy becomes $\partial_t(ne - nV) - \operatorname{div} S_n = W$. Thus, the convective terms disappear which is very useful for the design of numerical schemes.

The formulation (4)-(6) is not explicit in the macroscopic variables (n, ne) or (μ, T_n). Explicit expressions are obtained under simplifying assumptions. To this end, we approximate the Fermi-Dirac distribution by the Maxwellian $\exp(-(E-\mu)/T_n)$ and assume that the energy is given by the parabolic band approximation $E(k) = |k|^2/2$, that the elastic scattering rate is proportional to E^β with $\beta = 1/2$ (valid for nonpolar phonon scattering; see [35]), and that the averaged inelastic collision integral is approximated by a Fokker-Planck ansatz [21]. Then the energy-transport model consists of equations (4)-(5) with the relations

$$n = \frac{2}{(2\pi)^{3/2}} T^{3/2} e^{\mu/T_n}, \quad ne = \frac{3}{2} n T_n,$$

the (scalar) diffusion coefficients

$$D_{00} = \mu_0 n, \quad D_{01} = D_{10} = \frac{3}{2}\mu_0 n T_n, \quad D_{11} = \frac{15}{4}\mu_0 n T_n^2,$$

with the mobility constant $\mu_0 > 0$, and the relaxation-time term $W = -(3/2)n(T_n - T_L)/\tau$, where T_L is the lattice temperature and $\tau > 0$ is the energy relaxation time appearing in the Fokker-Planck ansatz. The current densities (5) can be written in the "drift-diffusion" form

$$J_n = \mu_0(\nabla n - n T_n^{-1} \nabla V), \quad S_e = \frac{3}{2}\mu_0(\nabla(nT_n) - n\nabla V). \tag{10}$$

The drawback of this formulation, compared to the "symmetric" form (9), is that the equations are convection dominated for large electric fields, which requires special numerical schemes. On the other hand, the model is decoupled in the "drift-diffusion" formulation, i.e., there are no cross-diffusion terms like in the formulation (5) or (9), which makes it easier to devise iteration schemes for the numerically discretized system.

We remark that there are also other energy-transport models in the literature which are different in the choice of the energy band and the definition of the scattering rate. For instance, the case $\beta = 0$ was considered in [36]. If $\beta = -1$, the model corresponds to some simplified hydrodynamic equations [33]. Nonparabolic energy bands were assumed in [17, 21, 51].

2.2 Numerical approximation

The numerical discretization of (stationary) energy-transport models was investigated in the physical literature since the 1980s, see, e.g., [17, 25, 44]. Mathematicians started to consider these models in the 1990s, using finite-difference methods [41], mixed finite-volume schemes [8], and mixed finite-element techniques [21, 27, 31, 32, 34, 37] (see [10] for a review). The most important features of the mixed finite-element method are the current conservation (the current is introduced as an independent variable and continuity is directly imposed) and the ability to approximate accurately steep gradients. In the following, we describe two approaches.

The approximation of [21, 31, 32] is based on the "drift-diffusion" formulation (10), which allows for the use of well-understood discrete schemes developed originally for the drift-diffusion model. The stationary equations are written in the form

$$-\operatorname{div} J + \sigma g = f, \quad J = \nabla g - \frac{\nabla V}{T_n} g, \tag{11}$$

where J is a current density, g the variable at hand, σg with $\sigma \geq 0$ is a zeroth-order term originating from the relaxation-time term in (4), and f is the right-hand side. In [31], the equation is discretized in two space dimensions as follows.

First, the problem is written by means of a local Slotboom variable in a symmetric form, defining $y = \exp(-V/\overline{T}_n)g$ in each element of the triangulation of the semiconductor domain, where $\overline{T}_n$ is some piecewise constant function approximating the electron temperature T_n. Then, the current density becomes $J = \exp(-V/\overline{T}_n)\nabla y$ in each element, which eliminates the drift term $g\nabla V/T_n$. This change of unknowns is also called exponential fitting.

In the second step, the symmetric form is discretized with mixed finite elements. For the case $\sigma = 0$ and constant temperature, a mixed scheme, based on the lowest-order Raviart-Thomas elements [40], has been introduced and discussed in [12] for $f = 0$ and in [11] for $f \neq 0$. The matrix associated with the scheme can be proved to be an M-matrix if a weakly acute triangulation is used. This property guarantees a discrete maximum principle and, in particular, a nonnegative solution if the boundary data are nonnegative. Unfortunately, the M-matrix property does not hold anymore if $\sigma \neq 0$. In order to circumvent this fact we use the finite elements developed and analyzed by Marini and Pietra [39]. It has been proved that these elements provide an M-matrix for all $\sigma \geq 0$.

In the third step, a suitable discrete change of unknowns is performed to return to the original variable g. Finally, static condensation gives a nonlinear discrete system only in the (discrete version of the) variable g. The nonlinear problem is solved by a variant of the Gummel iteration procedure. The main idea is to solve the Poisson equation, in which n and p are replaced by the local V-dependent Slotboom variables, by a Newton method, but to employ a fixed-point strategy for the remaining equations. It is well known that a Gummel-type iteration scheme is very sensitive to the choice of initial guess, in particular far from thermal equilibrium. Therefore, the procedure is coupled with a continuation in the applied voltage. In [32], the two-dimensional mesh is adaptively refined using an error estimator motivated by results of Hoppe and Wohlmuth.

As a numerical example, we simulate a two-dimensional MOSFET (metal-oxide semiconductor field-effect transistor) which can be employed as a voltage switch. It is the most used device in computer technology. The transistor has a size of $420\,\mathrm{nm} \times 210\,\mathrm{nm}$ with an effective channel (source to drain) length of $70\,\mathrm{nm}$

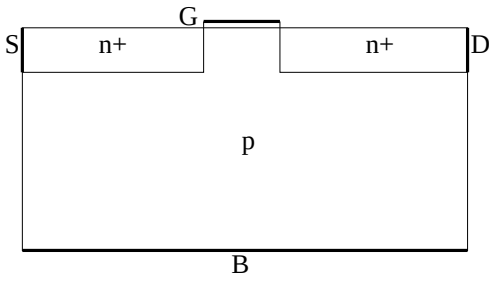

Figure 2: Geometry of the MOSFET with source *S*, drain *D*, gate *G*, and bulk *B* contacts.

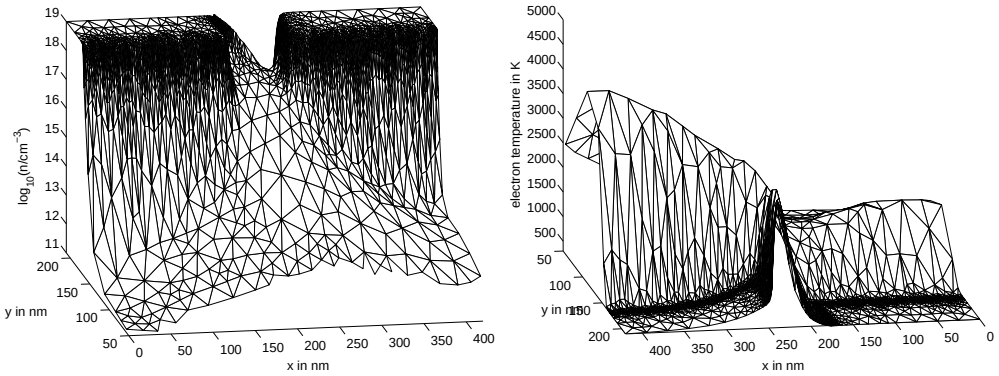

Figure 3: Electron density (left, gate contact at the back) and electron temperature (right, gate contact at the front) in a MOSFET with 70 nm channel length. A part of the bulk region is not shown.

and an oxide thickness of 1.5 nm near the gate contact (see Figure 2). For the physical parameters, we refer to [32] from which the following pictures are taken. The transistor is simulated using the energy-transport equations for electrons and the drift-diffusion equations for holes.

The electron density and temperature are shown in Figure 3. Close to the gate contact in the channel region, the electron density is large compared to the bulk density. In this region, the electron temperature is high too. The temperature near the the drain junction is larger than at the source junction since the electrons gain more energy from the electric field during their flow through the device.

The second numerical approach, employed in [27, 37], is based on the dual-entropy formulation (9). Compared to the previous approach, no convective terms appear, and the use of Raviart-Thomas-type mixed finite elements is sufficient to guarantee a monotone scheme. In [27], the three-dimensional stationary equations were approximated using a hybridized mixed finite element method with Raviart-Thomas-Nédélec elements. As above, static condensation allows for a reduction of the number of variables in the mixed-hybrid formulation. The resulting nonlinear algebraic system is solved by two iterative schemes, either using the full Newton method with a continuation in the applied voltage and a path-following algorithm or a Gummel-type strategy, which allows for a complete decoupling of the diffusion system such that only scalar equations have to be solved in each step. Since Gummel-type iteration procedures have a low convergence rate, a vector extrapolation technique was employed to improve the convergence.

As an example, we consider a unipolar nonuniform single-gate MESFET (metal-semiconductor field-effect transistor) with size $1\,\mu\text{m}\times 0.55\,\mu\text{m}\times 0.42\,\mu\text{m}$ (see Figure 4). The electron temperature is depicted in Figure 5 (left; taken from [27]). The temperature is large at the end of the channel since the kinetic energy of the electrons gained in the channel is transformed into thermal energy. The current flow is large in the region between the source and gate contact due to acceleration of the electrons from the electric field (see Figure 5, right).

In the above simulations, the device temperature is kept constant. We expect that collisions of high-energetic electrons with the crystal lattice increase the lattice temperature. In the following section, we present a model which couples the lattice and the particle temperatures.

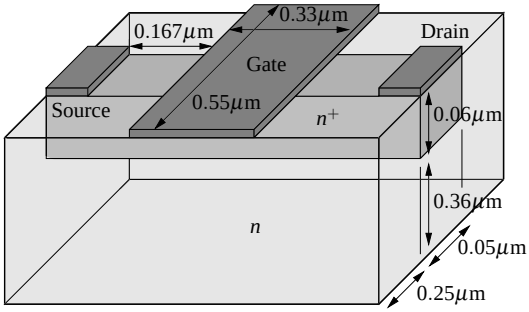

Figure 4: Geometry of the three-dimensional single-gate MESFET.

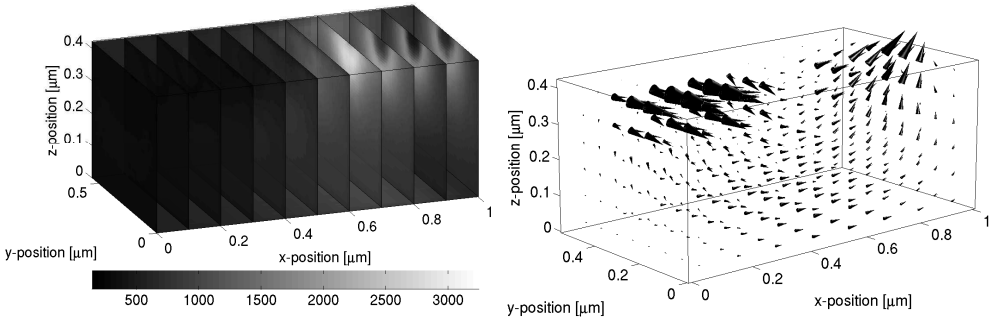

Figure 5: Electron temperature (left) and electron current density (right) in a three-dimensional single-gate MESFET.

3 Lattice heat modeling

We derive a model for the evolution of the lattice temperature T_L by employing thermodynamic principles, similar as in [5]. To this end, we assume that the total energy u satisfies the balance equation $\partial_t u + \operatorname{div} J_u = -\gamma$, where J_u is the corresponding energy flux density and γ the radiation. In the following, the expressions for u, J_u, and γ are detailed. Analogous to [5], we define the (scaled) free energy as the sum of the electric energy and the thermal energies of the lattice, electrons, and holes:

$$f = \frac{\lambda^2}{2}|\nabla V|^2 + \rho T_L(\log T_L - 1) + n\big(T_n(\log n - 1) + E_c\big) + p\big(T_p(\log p - 1) - E_v\big),$$

where ρ is the product of the (scaled) lattice material density and heat capacity, and E_c and E_v denote the conduction and valence band-edge energies, respectively. For simplicity, we suppose that these energies are independent of the lattice temperature. By thermodynamics, the total internal energy u can be written as

$$u = f - T_n\frac{\partial f}{\partial T_n} - T_p\frac{\partial f}{\partial T_p} - T_L\frac{\partial f}{\partial T_L}. \tag{12}$$

The total energy flux J_u is assumed to be the sum of the displacement current, Fourier flux, the particle energy fluxes, the currents of the dissipated power, and the currents due to the band energies:

$$J_u = -\lambda\nabla\partial_t V - \kappa_L\nabla T_L - (S_n + S_p) + (J_n + J_p)V - (E_c J_n + E_v J_p), \tag{13}$$

where κ_L is the lattice heat conductivity. Inserting the free energy into (12) and using (13), a computation gives

$$0 = \partial_t u + \operatorname{div} J_u = \rho\partial_t T_L - \operatorname{div}(\kappa_L\nabla T_L) - H, \tag{14}$$

where

$$H = -W + R(n,p)\Big(E_c - E_v + \frac{3}{2}(T_n + T_p)\Big) + J_n\cdot\nabla E_c + J_p\cdot\nabla E_v - \gamma$$

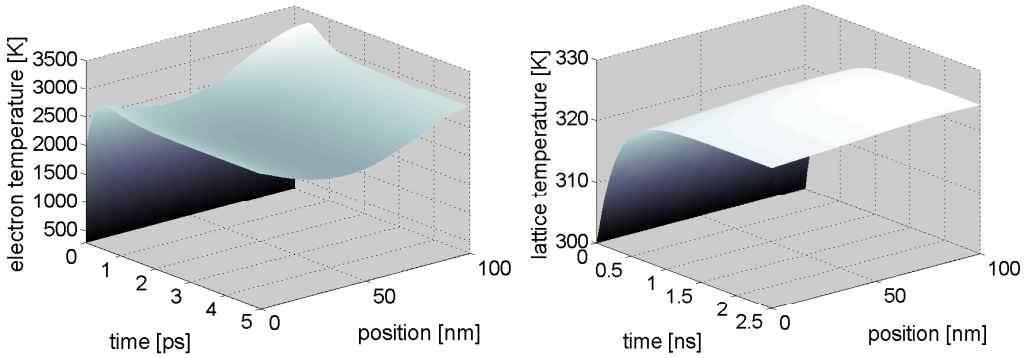

Figure 6: Transient electron temperature (left) and lattice temperature (right) in a *pn* diode at 1.5 V.

is the heat source term which is the sum of relaxation, recombination heat, band-energy Joule heating, and radiation effects. In [14], it is assumed that the band energies are homogeneous and that the radiation is linear in T_L such that

$$H = -W + R(n,p)\Big(E_c - E_v + \frac{3}{2}(T_n + T_p)\Big) - S_L(T_L - T_{\mathrm{env}}),$$

where S_L denotes the transmission constant and T_{env} the environmental temperature. This expression corresponds essentially to formula (41) in [50]. We remark that the expression for H differs from those in [5] and [49] since we take into account the evolution of the thermal energies of the particles via the energy-transport equations. When using a drift-diffusion model for the electrons, the Joule heating term $-J_n \cdot \nabla V$ has to be added to H (see [16]).

Equation (14) is complemented by an initial condition for T_L, homogeneous Neumann boundary conditions on the insulating boundary parts, and the Robin boundary condition

$$-\kappa_L \nabla T_L \cdot \nu = R_{\mathrm{th}}^{-1}(T_L - T_a) \quad \text{on } \Gamma_C, \tag{15}$$

where ν is the exterior unit normal vector on the domain boundary, Γ_C the union of all contacts, R_{th} the contact thermal resistance, and T_a the temperature of the connected element (the environmental temperature or the temperature of a circuit element).

We illustrate the transient lattice heating in a one-dimensional silicon bipolar junction diode (*pn* diode) with 100 nm length. The device is modeled by the bipolar energy-transport equations, coupled to the Poisson equation (8) and the lattice heat equation (14). Initially, the device is assumed to be in thermal equilibrium, i.e., the total current of electrons and holes vanishes. The transient response of the electron and lattice temperature is depicted in Figure 6 (taken from [16]). The electron temperature increases quickly in the entire device with a temperature maximum of about 3300 K in the *n*-region and then decreases slightly until the steady state is reached with a temperature minimum around the junction. The increase of the lattice temperature is significantly slower with a maximum of 325 K at steady state. Due to the high thermal conductivity, the lattice temperature is almost constant in the device.

Semiconductor devices are usually part of an electric circuit. In the following section, a circuit model is detailed including semiconductor devices.

4 Circuit modeling

This section is concerned with the modeling of electric circuits containing semiconductor devices. To simplify the presentation, the circuit is assumed to contain, besides of the semiconductor devices, only (ideal) resistors, capacitors, inductors, and voltage and current sources. The circuit is modeled by employing modified nodal analysis [47, 48], whose basic tools are the Kirchhoff laws and the current-voltage characteristics of the basic elements. We replace the circuit by a directed graph with branches and nodes.

Branch currents, branch voltages, and node potentials (without the mass node) are introduced as (time-dependent) variables. Then the circuit can be characterized by the incidence matrix $A = (a_{ik})$ describing the node-to-branch relations, with

$$a_{ik} = \begin{cases} 1 & \text{if the branch } k \text{ leaves the node } i, \\ -1 & \text{if the branch } k \text{ enters the node } i, \\ 0 & \text{else.} \end{cases}$$

The network is numbered in such a way that the indidence matrix consists of the block matrices A_R, A_C, A_L, A_i, and A_v, where the index indicates the resistive, capacitive, inductive, current source, and voltage source branches, respectively. The semiconductor device is included into the network model employing the semiconductor incidence matrix $A_S = (a_{ik}^S)$ defined by

$$a_{ik}^S = \begin{cases} 1 & \text{if the current } j_k \text{ enters the circuit node } i, \\ -1 & \text{if the reference terminal is connected to the node } i, \\ 0 & \text{else.} \end{cases}$$

The current-voltage characteristics for the basic elements are given by

$$i_R = g_R(v_R), \quad i_C = \frac{dq_C}{dt}(v_C), \quad v_L = \frac{d\phi_L}{dt}(i_L),$$

where g_R denotes the conductivity of the resistor, q_C the charge of the capacitor, and ϕ_L the flux of the inductor. Moreover, i_α and v_α with $\alpha = R, C, L$, are the branch current vectors and branch voltage vectors for, respectively, all resistors, capacitors, and inductors.

Denoting by $i_s = i_s(t)$, $v_s = v_s(t)$ the input functions for the current and voltage sources, respectively, the Kirchhoff laws lead to the following system of differential-algebraic equations in the charge-oriented modified nodal approach [47]:

$$A_C \frac{dq_C}{dt}(A_C^\top e) + A_R g_R(A_R^\top e) + A_L i_L + A_v i_v + A_S j_S = -A_i i_s, \tag{16}$$

$$\frac{d\phi_L}{dt}(i_L) - A_L^\top e = 0, \quad A_v^\top e = v_s, \tag{17}$$

for the unknowns $e(t)$, $i_L(t)$, and $i_v(t)$, where $e(t)$ denotes the vector containing the node potentials. Equation (16) is the Kirchhoff current law for the complete circuit, where the current-voltage relations for the resistors and capacitors have been included. The first equation in (17) describes the voltage-current characteristic for the inductors, and the second equation determines the node potentials adjacent to the given voltage sources.

The circuit is coupled to the device through the semiconductor current j_S in (16), defined by

$$j_S = \int_\Gamma (J_n + J_p - \lambda \partial_t \nabla V) \cdot \nu ds, \tag{18}$$

where Γ is some contact (terminal), and through the boundary conditions for the electric potential, given by $V(t) = e_j(t) + V_{\text{bi}}$ if the terminal Γ is connected to the circuit node j. Here, e_j denotes the potential at the circuit node j and V_{bi} is the built-in potential determined by the doping profile and the intrinsic density (see formula (11) in [16]).

Equations (16)-(17) represent a system of differential-algebraic equations (DAEs). Under certain assumptions on the topology of the network, the (tractability) index of the system is at most two [46, 47]. Moreover, if the circuit does neither contain so-called LI-cutsets nor CV-loops with at least one voltage source, the index is at most one [46].

For the numerical integration of DAEs, Runge-Kutta methods or backward difference formulas (BDFs) can be employed. For Runge-Kutta methods applied to DAEs, we refer, e.g., to [30]. Only implicit Runge-Kutta schemes are feasible for DAEs, and stiffly accurate methods provide the best properties. Concerning BDF methods, k-step BDFs (with $k < 7$) for index-1 DAEs are feasible for sufficiently small time steps,

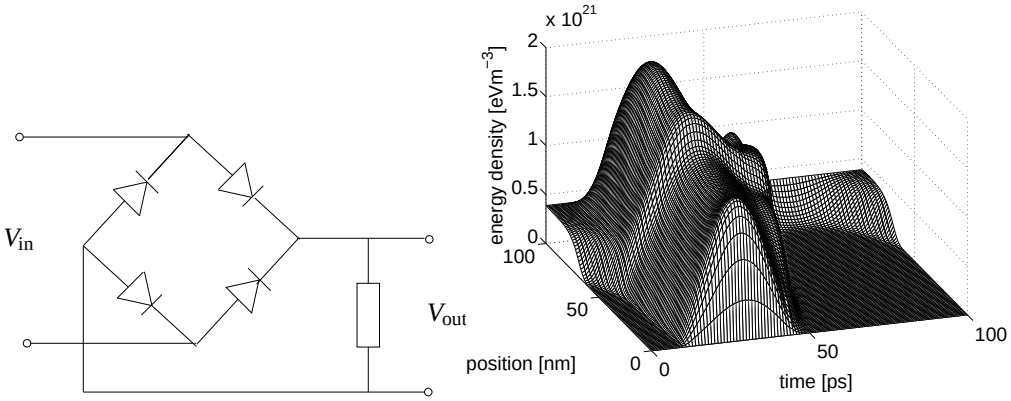

Figure 7: Rectifier circuit (left); energy density in a bipolar diode (right).

and they are convergent with the same order as in the case of explicit ordinary differential equations [38]. The numerical integration of index-2 DAEs with BDFs is studied in [9, 30]. In [46], quasilinear index-2 DAEs, as they occur in circuit simulation, were examined. We have employed the 2-step BDF method in the following simulations.

As an illustration, we consider a rectifier circuit modeled by the energy-transport equations for the electrons, the drift-diffusion equations for the holes, and the above circuit equations (presented first in [13]). After time discretization of the complete system, the particle transport equations are approximated by exponentially fitted hybrid-mixed finite elements as explained in Section 2.2. In this example, the lattice temperature is assumed to be constant but not the electron temperature. The circuit contains four *pn* diodes each of which with length 100 nm (see Figure 7, left). Initially, the system is assumed to be in thermal equilibrium. The voltage source is a sinusoidal signal with frequency 10 GHz.

In Figure 7 (right) the energy density in one of the diodes during one oscillation of the circuit is presented. The energy density is only significant in the forward biased cycle, whereas it is very small for backward bias.

Next, the behavior of the current through one diode and through the circuit using the transient or stationary energy-transport (ET) equations and the transient drift-diffusion (DD) model is investigated. Figure 8 (left) clearly shows the rectifying behavior of the circuit. We also observe a capacitive effect at this rather high frequency. The largest current is obtained from the drift-diffusion model since we have assumed a constant electron mobility such that the drift is unbounded with respect to the modulus of the electric field. The stationary energy-transport model is not able to catch the capacitive effect at the junction. Similar statements hold for the output signal of the circuit (Figure 8, right).

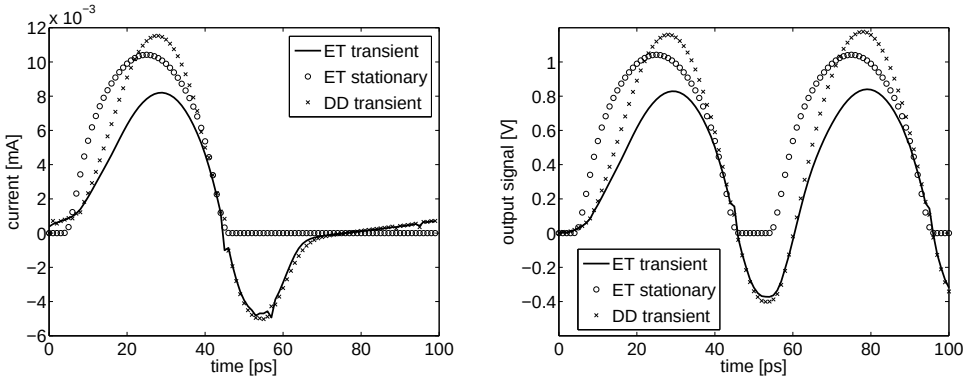

Figure 8: Current through a 0.1 μm diode in a 10 GHz circuit (left); output signal of the circuit (right).

5 Thermal network modeling

The thermal network describes how the heat is produced and how it is evolving in the circuit topology. To simplify the presentation, we consider only one semiconductor device in the network. Moreover, as a compromise between physical accuracy and fast numerical simulation, all thermally relevant elements in the circuit – except the semiconductor device – are modeled by zero- or one-dimensional structures.

We consider the following elements in the thermal network [6, 7]. Lumped thermal elements are zero-dimensional objects (for instance, resistors or contact nodes) to which a spatially constant temperature $\widehat{T}^\ell(t)$ is associated. Distributed thermal lines are modeled in one space dimension (for instance, electric lines or circuit elements) with an associated temperature $T^d(x,t)$, $x \in [0, L_{\text{th}}]$. Moreover, a distributed semiconductor device possesses the temperature $T_L(x,t)$ as described in Section 3. Adjacent lumped elements are considered as a zero-dimensional object with temperature $\widehat{T}$. Then we assign the temperature at the interface of connected distributed elements and an artificial zero-dimensional element (thermal node) with temperature $\widehat{T}$ and without thermal mass. This forms a network with lumped-distributed interfaces only, in which the nodes represent the zero-dimensional units and the branches represent the distributed elements.

The thermal network is characterized by the thermal incidence matrix $A_d^{\text{th}} = (a_{ij}^{\text{th}})$ and the thermal semiconductor incidence matrix $A_S^{\text{th}} = (a_{S,ij}^{\text{th}})$ defined by

$$a_{ij}^{\text{th}} = \begin{cases} 1 & \text{if the contact at } x = 0 \text{ of branch } j \text{ is connected to node } i, \\ 1 & \text{if the contact at } x = L_{\text{th}} \text{ of branch } j - m_d \text{ is connected to node } i, \\ 0 & \text{else,} \end{cases}$$

$$a_{S,ij}^{\text{th}} = \begin{cases} 1 & \text{if the terminal } j \text{ is connected to thermal node } i, \\ 0 & \text{else,} \end{cases}$$

where m_d is the number of thermal lines and $[0, L_{\text{th}}]$ the interval of the distributed element.

The temperature in the thermal nodes is supposed to evolve according to the heat equation

$$\widehat{M}\frac{d\widehat{T}}{dt} = \widehat{F}^d + \widehat{F}^S - \widehat{S}(\widehat{T} - T_{\text{env}} I) + \widehat{P}, \quad t > 0. \tag{19}$$

Here, $\widehat{M}$ is a diagonal matrix containing the thermal masses of the thermal nodes, each of which is given as the sum of the thermal masses of the lumped elements contributing to the corresponding node. The thermal mass is the product of the heat capacity, the material density, and the physical volume of the corresponding element. Furthermore, $\widehat{T}$ is the vector of all temperature values in the thermal nodes, and I is the identity matrix. The electro-thermal source vector for the thermal nodes $\widehat{P}$ and the heat flux vectors from the distributed lines $\widehat{F}^d$ and the device $\widehat{F}^S$ are defined below in (23), (21), and (22), respectively. The temperature values in the lumped elements $\widehat{T}^\ell$ can be computed from $\widehat{T}$ by the formula $\widehat{T} = M\widehat{T}^\ell$, where the matrix $M = (m_{ij})$ relates the lumped elements to the thermal nodes, with $m_{ij} = 1$ if the lumped element j belongs to the thermal node i and $m_{ij} = 0$ else.

The vector $T^d = (T_j^d)$ of all temperatures of the thermal lines satisfies

$$M_j \partial_t T_j^d = \partial_x(\kappa_j \partial_x T_j^d) - S_j(T_j^d - T_{\text{env}}) + P_j, \quad x \in (0, L_j),\ t > 0, \tag{20}$$

where M_j denotes the thermal mass of the j-th element of length L_j, κ_j is the thermal conductivity, S_j the transmission constant, and $P = (P_j)$ the electro-thermal source vector defined in (23). The above equation is complemented by initial conditions and Dirichlet boundary conditions, collected in the vectors T_0^d and T_1^d.

6 The fully coupled model

In this section, we explain the coupling conditions between the subsystems introduced in the previous sections and give a numerical example of the full coupled thermo-electric semiconductor-circuit system.

6.1 Coupling conditions

The heat equations (19) and (20) are coupled through the boundary conditions, $(T_0^d, T_1^d)^\top = (A_d^{\mathrm{th}})^\top \widehat{T}$, and the following equation for the thermal flux:

$$\widehat{F}^d = A_d^{\mathrm{th}} \begin{pmatrix} \Lambda_0 \partial_x T^d(0,t) \\ -\Lambda_1 \partial_x T^d(L_{\mathrm{th}},t) \end{pmatrix}. \tag{21}$$

Here, L_{th} denotes the length of a thermal line and Λ_0, Λ_1 contain the products of thermal conductivities and the cross sections of the thermal lines at $x = 0$ and $x = L_{\mathrm{th}}$, respectively.

Next, we describe the coupling between the thermal network and the semiconductor device. The influence of the network on the device is modeled by the boundary condition (15) on the terminal Γ_k, with T_{env} replaced by the temperature of the connected elements, $T_a = (A_S^{\mathrm{th}})^\top \widehat{T}$. The semiconductor heat flux at terminal Γ_k is given by the integral

$$F_k^S = \int_{\Gamma_k} J_{\mathrm{th}}^S \cdot \nu \, d\sigma, \quad \text{such that} \quad \widehat{F}^S(t) = A_S^{\mathrm{th}} (F_j^S(t))_j, \quad t > 0. \tag{22}$$

The thermal flux density J_{th}^S is derived by making the quasi-stationary assumption $\operatorname{div} J_u = 0$, where the energy flux density J_u is defined in (13). Then, inserting the stationary balance equation for the electric energy, a computation shows that, assuming a constant hole temperature,

$$\operatorname{div} J_{\mathrm{th}}^S + \nabla V \cdot (J_n + J_p) = 0, \quad \text{where} \quad J_{\mathrm{th}}^S = -\kappa_L \nabla T_L - E_c J_n - S_n$$

(see [14] for details). This equation indicates that the flux J_{th}^S is responsible for the heat production caused by the dissipated power and is therefore considered as a heat flux.

For the coupling between the electric and thermal network, we assume that only semiconductor devices and resistors are thermally relevant. (In the numerical simulation below, thermal effects in the resistor are neglected.) Electric-to-thermal coupling occurs through the power dissipated by a resistor. We assume that the resistance is given by $R = 1 + \alpha_1 T_R + \alpha_2 T_R^2$, where α_1 and α_2 are some nonnegative parameters and T_R is the temperature of the resistor [6]. The vector T_R of all resistor temperature values can be determined from the temperature vectors of the thermal nodes $\widehat{T}$ and of the distributed lines T^d by

$$T_R = \widehat{K}^\top \widehat{T} + K^\top \widetilde{T}^d,$$

where the lumped values $\widetilde{T}^d$ are computed from the distributed values T^d by taking the mean value, and the matrices $K = (k_{\ell j})$ and $\widehat{K} = (\widehat{k}_{\ell j})$ are defined by

$$k_{\ell j} = \begin{cases} 1 & \text{if the resistor } j \text{ corresponds to the thermal branch } \ell, \\ 0 & \text{else,} \end{cases}$$

$$\widehat{k}_{\ell j} = \begin{cases} 1 & \text{if the resistor } j \text{ corresponds to the thermal node } \ell, \\ 0 & \text{else.} \end{cases}$$

The electric-to-thermal coupling is realized by the source terms $P = (P_j)$ and $\widehat{P}$ in the heat equations (19) and (20):

$$\widehat{P} = \widehat{K} P_R, \quad P = L_R^{-1} K P_R, \quad \text{where } P_R = \operatorname{diag}(i_R) A_R^\top e, \tag{23}$$

i_R contains the currents through all resistors, A_R denotes the resistor incidence matrix, e is the vector containing the node potentials, and L_R is the resistor length. For a discussion about the proper choice of the local power distribution, we refer to [6].

Finally, we recall that the coupling between the semiconductor device and the electric circuit is realized through the semiconductor current (18) in the circuit equation (16) and the node potentials applied to the semiconductor contacts.

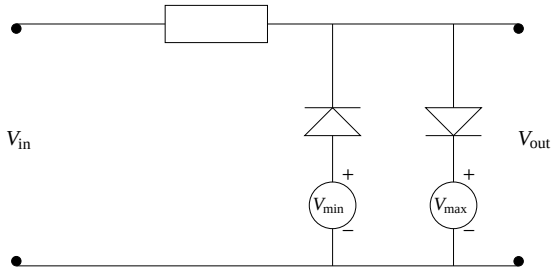

Figure 9: Clipper circuit with two *pn* diodes, one resistor, and three voltages sources.

6.2 Numerical example

The complete thermo-electric circuit-semiconductor model is a system of nonlinear partial differential-algebraic equations. It consists of the energy-transport equations (4), (10) for the electrons, the drift-diffusion equations (7) for the holes (alternatively, energy-transport equations for the holes may be used), the Poisson equation (8); the differential algebraic electric network equations (16)-(17); and the thermal network equations (19)-(21). The coupling conditions are given in (18) and (22)-(23). The unknowns of the system are the electron, energy and hole densities, n, ne, p, the potential in the device V, the node potentials e, the currents through inductors, voltage sources, and semiconductor device, i_L, i_V, j_S, the lattice temperature T_L, and the temperature values in the lumped and distributed elements of the thermal network, $\widehat{T}$, T^d.

As a numerical illustration, we consider a clipper which is employed as an entrance protective circuit to avoid voltage peaks (taken from [16]). It consists of two *pn* diodes (modeled in one space dimension), one resistor, and three voltage sources (see Figure 9). We concentrate on the effect of lattice heating and neglect thermal effects in the resistor. The sinusoidal input signal V_{in} has a frequency of 10 GHz. The remaining voltages are kept constant with $V_{\text{min}}(t) = -U$ and $V_{\text{max}}(t) = U$, where $U = 2\,\text{V}$. A perfect clipper restricts the input signal between $\pm(U + V_{\text{th}})$, where V_{th} is the threshold voltage of the diode. In the present case, it holds approximately $V_{\text{th}} = 0.9\,\text{V}$ such that the signal is between $\pm 2.9\,\text{V}$. We have chosen the resistance such that the output signal should stay below 4 V.

In Figure 10 (left) we depict the input and output signals of the circuit after 30 oscillations of V_{in}. Whereas the maximal output signal is below 4 V during the first oscillations, it becomes 4.09 V after 30 oscillations. A simulation of the same circuit with constant lattice heating keeps the maximum output signal below 4 V. This shows that the increasing maximal output voltage is caused by lattice heating, as the heated diode provides less current leading to a larger resistance. We observe from Figure 10 (right) that the device heats up while being forward biased. As the backward bias period is too short to cool down the device, the lattice heating accumulates during the first oscillations up to about 360 K.

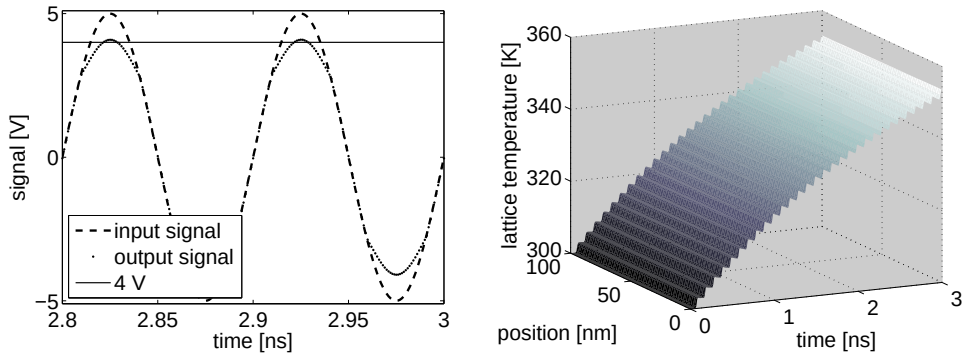

Figure 10: Input and output signal of the clipper after 30 oscillations of V_{in} (left) and distribution of the lattice temperature in one of the diodes within the first 30 oscillations of V_{in} (right).

Acknowledgements

The author acknowledges partial support from the Austrian Science Fund (FWF), grant P20214 and WK "Differential Equations", from the German Science Foundation (DFG), grant JU 359/7, and from the German-French DAAD-Procope Program. This research is part of the ESF program "Global and geometrical aspects of nonlinear partial differential equations (GLOBAL)".

7 References

[1] M. Adler. Accurate calculations of the forward drop and power dissipation in thyristors. *IEEE Trans. Electr. Dev.* 25 (1978), 16-22.

[2] G. Albinus, H. Gajewski, and R. Hünlich. Thermodynamic design of energy models of semiconductor devices. *Nonlinearity* 15 (2002), 367-383.

[3] G. Alì and M. Carini. Energy-transport models for semiconductor devices and their coupling with electric networks. In: V. Cutello, G. Fotia, L. Puccio (eds.), *Applied and Industrial Mathematics in Italy II*, 13-24. World Scientific Publ., New Jersey, 2007.

[4] W. Allegretto and H. Xie. Nonisothermal semiconductor systems. In: X. Liu and D. Siegel (eds.), *Comparison Methods and Stability Theory*. Lecture Notes Pure Appl. Math. 162, 17-24. Marcel Dekker, New York, 1994.

[5] U. Bandelow, H. Gajewski, and R. Hünlich. Fabry-Perot lasers: thermodynamic-based modeling. In: *Optoelectronic Devices. Advanced Simulation and Analysis*, J. Piprek (ed.), 63-85. Springer, Berlin, 2005.

[6] A. Bartel. *Partial Differential-Algebraic Models in Chip Design – Thermal and Semiconductor Problems*. Ph.D. thesis, Universität Karlsruhe, Germany, 2003.

[7] A. Bartel and M. Günther. From SOI to abstract electric-thermal-1D multiscale modeling for first order thermal effects. *Math. Comput. Modell. Dynam. Syst.* 9 (2003), 25-44.

[8] F. Bosisio, R. Sacco, F. Saleri, and E. Gatti. Exponentially fitted mixed finite volumes for energy balance models in semiconductor device simulation. In: H. Bock et al. (eds.), *Proceedings of ENUMATH 97*, 188-197. World Scientific, Singapore, 1998.

[9] K. Brennan, S. Campell, and L. Petzold. *Numerical Solution of Initial-Value Problems in Differential-Algebraic Equations*. North-Holland, New York, 1989.

[10] F. Brezzi, L. Marini, S. Micheletti, P. Pietra, R. Sacco, and S. Wang. Discretization of semiconductor device problems. In: W. Schilders and E. ter Maten, *Handbook of Numerical Analysis, Vol. 13: Numerical Methods in Electromagnetics*, 317-441. North-Holland, Amsterdam, 2005.

[11] F. Brezzi, L. Marini, and P. Pietra. Numerical simulation of semiconductor devices. *Comput. Methods Appl. Mech. Engrg.* 75 (1989), 493-514.

[12] F. Brezzi, L. Marini, and P. Pietra. Two-dimensional exponential fitting and applications to drift-diffusion models. *SIAM J. Numer. Anal.* 26 (1989), 1342-1355.

[13] M. Brunk and A. Jüngel. Numerical coupling of electric circuit equations and energy-transport models for semiconductors. *SIAM J. Sci. Comput.* 30 (2008), 873-894.

[14] M. Brunk and A. Jüngel. Self-heating in a coupled thermo-electric circuit-device model. Submitted for publication, 2009.

[15] M. Brunk and A. Jüngel. Simulation of thermal effects in optoelectronic devices using coupled energy-transport and circuit models. *Math. Models Meth. Appl. Sci.* 18 (2008), 1-26.

[16] M. Brunk and A. Jüngel. Heating of semiconductor devices in electric circuits. To appear in *Proceedings of the Conference on Scientific Computing in Electrical Engineering (SCEE 2008)*, 2009.

[17] D. Chen, E. Kan, U. Ravaioli, C. Shu, and R. Dutton. An improved energy transport model including nonparabolicity and non-Maxwellian distribution effects. *IEEE Electr. Device Letters* 13 (1992), 26-28.

[18] L. Chen, L. Hsiao, and Y. Li. Large time behavior and energy relaxation time limit of the solutions to an energy transport model in semiconductors. *J. Math. Anal. Appl.* 312 (2005), 596-619.

[19] P. Degond, S. Génieys, and A. Jüngel. A system of parabolic equations in nonequilibrium thermodynamics including thermal and electrical effects. *J. Math. Pures Appl.* 76 (1997), 991-1015.

[20] P. Degond, S. Génieys, and A. Jüngel. A steady-state system in nonequilibrium thermodynamics including thermal and electrical effects. *Math. Meth. Appl. Sci.* 21 (1998), 1399-1413.

[21] P. Degond, A. Jüngel, and P. Pietra. Numerical discretization of energy-transport models for semiconductors with nonparabolic band structure. *SIAM J. Sci. Comput.* 22 (2000), 986-1007.
[22] P. Degond, C. Levermore, and C. Schmeiser. A note on the energy-transport limit of the semiconductor Boltzmann equation. In: N. Ben Abdallah et al. (eds.), *Proceedings of Transport in Transition Regimes* (Minneapolis, 2000), IMA Math. Appl. 135, 137-153. Springer, New York, 2004.
[23] K. Einwich, P. Schwarz, P. Trappe, and H. Zojer. Simulatorkopplung für den Entwurf komplexer Schaltkreise der Nachrichtentechnik. In: 7. ITG-Fachtagung "Mikroelektronik für die Informationstechnik", Chemnitz (1996), 139-144.
[24] W. Fang and K. Ito. Existence of stationary solutions to an energy drift-diffusion model for semiconductor devices. *Math. Models Methods Appl. Sci.* 11 (2001), 827-840.
[25] A. Forghieri, R. Guerrieri, P. Ciampolini, A. Gnudi, M. Rudan, and G. Baccarani. A new discretization strategy of the semiconductor equations comprising momentum and energy balance. *IEEE Trans. Computer-Aided Design Integr. Circuits Sys.* 7 (1988), 231-242.
[26] K. Fukahori. *Computer Simulation of Monolithic Circuit Performance in the Presence of Electrothermal Interactions*. Ph.D. thesis, University of California, Berkeley, USA, 1977.
[27] S. Gadau and A. Jüngel. A three-dimensional mixed finite-element approximation of the semiconductor energy-transport equations. *SIAM J. Sci. Comput.* 31 (2008), 1120-1140.
[28] J. Griepentrog. An application of the implicit function theorem to an energy model of the semiconductor theory. *Z. Angew. Math. Mech.* 79 (1999), 43-51.
[29] S. de Groot and P. Mazur. *Nonequilibrium Thermodynamics*. Dover Publications, New York, 1984.
[30] E. Hairer and G. Wanner. *Solving Ordinary Differential Equations II*. Springer, Berlin, 1991.
[31] S. Holst, A. Jüngel, and P. Pietra. A mixed finite-element discretization of the energy-transport equations for semiconductors. *SIAM J. Sci. Comput.* 24 (2003), 2058-2075.
[32] S. Holst, A. Jüngel, and P. Pietra. An adaptive mixed scheme for energy-transport simulations of field-effect transistors. *SIAM J. Sci. Comput.* 25 (2004), 1698-1716.
[33] A. Jüngel. *Transport Equations for Semiconductors*. Lecture Notes in Physics 773. Springer, Berlin, 2009 (to appear).
[34] C. Lab and P. Caussignac. An energy-transport model for semiconductor heterostructure devices: Application to AlGaAs/GaAs MODFETs. *COMPEL* 18 (1999), 61-76.
[35] M. Lundstrom. *Fundamentals of Carrier Transport.* 2nd edition, Cambridge University Press, Cambridge, 2000.
[36] E. Lyumkis, B. Polsky, A. Shur, and P. Visocky. Transient semiconductor device simulation including energy balance equation. *COMPEL* 11 (1992), 311-325.
[37] A. Marrocco and P. Montarnal. Simulation de modèles "energy transport" à l'aide des éléments finis mixtes. *C. R. Acad. Sci. Paris, Sér. I* 323 (1996), 535-541.
[38] R. März. Numerical methods for differential-algebraic equations. *Acta Numer.* 1 (1992), 141-198.
[39] L. Marini and P. Pietra. New mixed finite element schemes for current continuity equations. *COMPEL* 9 (1990), 257-268.
[40] P. Raviart and J. Thomas. A mixed finite element method for second order elliptic equations. In: *Mathematical Aspects of the Finite Element Method* (Proc. Conf. Rome 1975), *Lecture Notes in Math.* 606, 292-315. Springer, New York, 1977.
[41] C. Ringhofer. An entropy-based finite difference method for the energy transport system. *Math. Models Meth. Appl. Sci.* 11 (2001), 769-796.
[42] M. Rudan, A. Gnudi, and W. Quade. A generalized approach to the hydrodynamic model of semiconductor equations. In: G. Baccarani (ed.), *Process and Device Modeling for Microelectronics*, 109-154. Elsevier, Amsterdam, 1993.
[43] M. Selva Soto and C. Tischendorf. Numerical analysis of DAEs from coupled circuit and semiconductor simulation. *Appl. Numer. Math.* 53 (2005), 471-488.
[44] K. Souissi, F. Odeh, H. Tang, and A. Gnudi. Comparative studies of hydrodynamic and energy transport models. *COMPEL* 13 (1994), 439-453.
[45] R. Stratton. Diffusion of hot and cold electrons in semiconductor barriers. *Phys. Rev.* 126 (1962), 2002-2014.
[46] C. Tischendorf. Topological index calculation of differential-algebraic equations in circuit simulation. *Surv. Math. Industr.* 8 (1999), 187-199.
[47] C. Tischendorf. *Coupled Systems of Differential Algebraic and Partial Differential Equations in Circuit and Device Simulations*. Habilitation thesis, Humboldt-Universität zu Berlin, Germany, 2003.

[48] C. Tischendorf. Modeling circuit systems coupled with distributed semiconductor equations. In: K. Antreich, R. Bulirsch, A. Gilg, and P. Rentrop (eds.), *Modeling, Simulation, and Optimization of Integrated Circuits*, *Internat. Ser. Numer. Math.* 146 (2003), 229-247.

[49] G. Wachutka. Rigorous thermodynamic treatment of heat generation and conduction in semiconductor device modeling. *IEEE Trans. Comp. Aided Design* 9 (1990), 1141-1149.

[50] G. Wachutka. Consistent treatment of carrier emission and capture kinetices in electrothermal and energy transport models. *Microelectr. J.* 26 (1995), 307-315.

[51] D. Woolard, H. Tian, R. Trew, M. Littlejohn, and K. Kim. Hydrodynamic electron-transport: Non-parabolic corrections to the streaming terms. *Phys. Rev. B* 44 (1991), 11119-11132.